

# Learning Motion Predictors for Smart Wheelchair using Autoregressive Sparse Gaussian Process

Zicong Fan<sup>1</sup>, Lili Meng<sup>1</sup>, Tian Qi Chen<sup>3</sup>, Jingchun Li<sup>1</sup> and Ian M. Mitchell<sup>1</sup>  
The University of British Columbia, Vancouver, Canada

**Abstract**— Constructing a smart wheelchair on a commercially available powered wheelchair (PWC) platform avoids a host of seating, mechanical design and reliability issues but requires methods of predicting and controlling the motion of a device never intended for robotics. Analog joystick inputs are subject to black-box transformations which may produce intuitive and adaptable motion control for human operators, but complicate robotic control approaches; furthermore, installation of standard axle mounted odometers on a commercial PWC is difficult. In this work, we present an integrated hardware and software system for predicting the motion of a commercial PWC platform that does not require any physical or electronic modification of the chair beyond plugging into an industry standard auxiliary input port. This system uses an RGB-D camera and an Arduino interface board to capture motion data, including visual odometry and joystick signals, via ROS communication. Future motion is predicted using an autoregressive sparse Gaussian process model. We evaluate the proposed system on real-world short-term path prediction experiments. Experimental results demonstrate the system’s efficacy when compared to a baseline neural network model.

## I. INTRODUCTION

It is estimated that by the year 2050 the number of people over the age of 85 will have tripled [6], and a significant portion of the aging population is expected to need mobility assistance. Confidence in independent mobility is core to psychological functioning [1], and a greater sense of control can be positively correlated with a reduced mortality rate; consequently, the ability of powered wheelchairs (PWCs) to provide improved mobility could lead to a host of positive outcomes for this growing but mobility challenged population. Unfortunately, older adults often have sensory, motor and/or cognitive impairments that preclude them from safely operating these large, heavy and powerful machines [11].

Smart wheelchairs (SWCs) seek to overcome the limitation of PWCs by using sensing, planning and control techniques from the robotics community to ensure safe operation and support the operator to accomplish tasks of daily living. Constructing the “smarts” as an add-on to a commercially available PWC platform avoids a host of seating, mechanical

design and reliability issues, but requires methods of predicting and controlling the motion of a device that was never intended for robotics. Although commercial PWCs use power electronics, control systems, communication buses and input devices from several companies, the leading manufacturers consider their technical specifications and interfaces proprietary. Furthermore, modifications to mobility critical aspects of the PWC, such as the drive train, are impractical because of their complexity and the risk of a failure stranding the driver; consequently, it is not possible to get wheel odometry by mounting sensors on the drive wheel’s axle.

These complications mean that the basic capabilities assumed by most algorithms for wheeled robots—estimating what path the robot will take based on what motion commands were given, and estimating what motion commands will lead the robot along a particular path—are difficult to achieve on commercial PWC platforms.

In order to capitalize on the autonomous motion techniques developed by the robotics community and thereby turn a PWC into a SWC, we propose to provide these basic prediction capabilities using a combination of visual odometry, a standard analog “alternative input” port on the PWC and autoregressive sparse Gaussian process models. The visual odometry is obtained through a low-cost, lightweight and discretely mounted RGB-D camera. An Arduino board with a simple custom shield card provides the interface between the PWC and a laptop running ROS. We evaluate the system in real-world environments, including different floor and lighting conditions. Experimental results demonstrate the efficacy of our estimates. Because this infrastructure can be easily ported to a wide variety of PWC bases from different manufacturers and integrated with a wide variety of sensing and planning technology available in ROS, we believe it represents a significant step toward bringing SWC autonomy into the PWC marketplace.

## II. RELATED WORK

### A. Smart Powered Wheelchairs

Research on SWCs has a long history and is still an active area. An early survey can be found in [24], so here we constrain the discussion to some recent work. In [8] the authors take a Bayesian approach to learning the user model simultaneously with a dialog manager policy for intelligent planning. PerMMA [5] combines manipulation and mobility

This work was supported by AGE-WELL NCE Inc. (a member of the Canadian Networks of Centres of Excellence program) and the National Science and Engineering Research Council of Canada (NSERC) Discovery Grant #298211.

<sup>1</sup>Zicong Fan, Lili Meng, Jingchun Li and Ian M. Mitchell are with the Department of Computer Science at The University of British Columbia in Vancouver, Canada. zfan@alumni.ubc.ca, menglili@cs.ubc.ca, mitchell@cs.ubc.ca

<sup>3</sup>Tian Qi Chen is with the Department of Computer Science at the University of Toronto in Toronto, Canada. rtqichen@cs.toronto.edu

assistance in support of complete independence for its users. A wizard of oz experiment was used in [27] to explore SWC control strategies for older adults with cognitive impairment, including user attitudes, needs, and preferences. Seating pressure sensors are used to monitor the user in [17]. An assessment of driving assistance by a deictic command for an SWC is proposed in [15], which enables the user to indicate desired motion on an interface displaying a view of the environment. An SWC capable of autonomous navigation in urban environments which integrates 3D perception is developed in [22]. However, all of this work has focused on other features of an SWC, such as autonomous navigation, collision avoidance or detection of abnormal user behavior; little work as been focused on motion prediction for general PWC platforms.

### B. Visual Odometry

Visual odometry (VO) is the process of estimating the ego-motion of an agent using as a measurement input the images from cameras attached to it. Compared with wheel odometry, VO is not affected by the wheel slip common in uneven terrain or slippery environments. It has been demonstrated that VO can generate more accurate trajectory estimates than wheel odometry, with relative position error ranging from 0.1% to 2% [21]. Sparse feature-based methods [20], [12] and dense photometric-error based methods [13] are two widely used methods for VO. The former are based on salient and repeatable features that are tracked over the frames, while the latter use the intensity information of all the pixels in the image. In this work, we take advantage of the sparse feature-based VO package Fovis [12]. Fovis is compared with five other VO algorithms (including DVO [13] and GICP [23]) in [10] and is shown to have just half the runtime and half the average CPU usage; additionally, it performed best among the algorithms on “Test2” involving complex environments with long corridors and cluttered or spacious rooms.

### C. Learning Robot Motion Models

Machine learning methods have been widely applied to robotics tasks such as manipulation [16], autonomous driving [2] and localization [18], and we propose to similarly learn the motion model. This exact problem was studied in [26], which built a simple feed-forward neural network with a single hidden layer and only first-order differential information from the joystick and odometry readings. A more complex probabilistic odometry model from input commands is presented in [9], but their motion model is mainly developed for use in a simultaneous localization and mapping (SLAM) algorithm. An FCN-LSTM architecture is used in [28] to learn a driving model from a large scale outsourced video dataset with GPS labels; however, it uses manual labeling and GPS signals only available in outdoor driving scenarios, while our focus remains on the indoor environments more frequently encountered by older adults.

## III. THE PWC HARDWARE AND SOFTWARE PLATFORM

The main hardware components of our platform are shown in Fig. 1. The PWC is an off-the-shelf commercial Permobil M300 corpus 3G. The PWC’s built-in joystick is overridden through an Rnet Omni+ alternative input device port into which we can plug a Penny & Giles JC 200 joystick. To intercept and/or modify the joystick signal, we use a custom analog interface board attached as a shield to an Arduino Mega single board microcontroller. The custom board can read the analog joystick and write signals that look like the analog joystick’s signals to the Omni+ input device port. The board is controlled by the Arduino, which in turn communicates through a serial port with a Lenovo W530 laptop (Intel Core i7 with 8GB memory) running ROS. An Asus Xtion RGB-D camera is mounted looking backwards behind the seat to avoid interference with the driver and to reduce the aesthetic impact. The camera can deliver RGB frames at 30Hz and depth images with 640x480 resolution and 58 HFV.

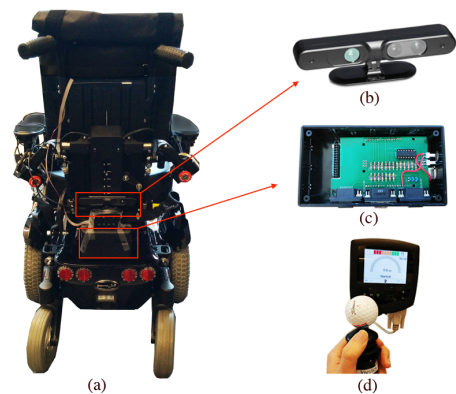


Fig. 1: **PWC hardware platform.** (a) The back view of our PWC. RGB-D sensor is mounted at the back of the PWC. (b) An ASUS Xtion RGB-D camera used to capture the visual odometry data. (c) Arduino control box (opened to show contents). (d) A JC200 analog joystick used to control the PWC through the R-net Omni+ alternative input port.

Fig. 2 (a) shows how the hardware components interact:

- The joystick sends the control signal to the Arduino box.
- The Arduino box passes the control messages to the laptop running ROS.
- The Arduino box also passes the same control signal to the PWC to override the built-in joystick (shown in the dashed box).
- The RGB-D camera passes images to the laptop.

The software pipeline is shown in Fig. 2 (b). During data collection the joystick and VO data on the indicated ROS topics are stored to a bag file on the laptop. After collection the data are resampled using interpolation onto a common 5Hz frequency, and the resampled data is used to train or test the motion prediction model.

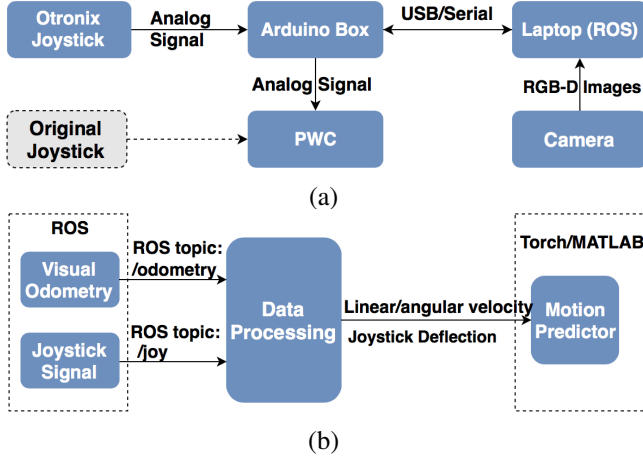


Fig. 2: **Our communication pipelines.** (a) Hardware pipeline, (b) Software pipeline.

#### IV. AUTOREGRESSIVE SPARSE GAUSSIAN PROCESSES

In this section, we introduce our autoregressive sparse Gaussian process model for motion prediction. While our end goal is pose trajectory, VO provides velocity data so we will estimate the velocity sequence and integrate to find pose trajectory.

We denote an element of our time series by the joystick and velocity pair  $(J_t, V_t) \in \mathbb{R}^4$ , where  $J_t \in \mathbb{R}^2$  and  $V_t \in \mathbb{R}^2$  represent the joystick deflections and velocity at time step  $t$  respectively. The components of  $J_t$  are the forward-backward deflection (intuitively the linear velocity command) and leftward-rightward deflection (intuitively the angular velocity command). The components of  $V_t$  are linear and angular velocity measurements which we will denote as  $[v_t, \omega_t]^T$ . Inspired by the time series autoregressive process [3], we use the past  $s$  time-steps of the time series as the input to predict the current time-step  $(J_t, V_t)$ . In fact, because we are concerned only with velocity prediction, we also provide the current joystick  $J_t$  to our prediction function. Defining

$$\begin{aligned} X_t &= \{\bar{X}_t, J_t\}, \\ \bar{X}_t &= [J_{t-s}, \dots, J_{t-1}, V_{t-s}, \dots, V_{t-1}]^T, \end{aligned}$$

we can for notational convenience write our prediction function in several different ways:

$$\begin{aligned} \hat{V}_t &= f(J_{t-s}, \dots, J_{t-1}, V_{t-s}, \dots, V_{t-1}, J_t), \\ &= f(\bar{X}_t, J_t), \\ &= f(X_t), \\ V_t &= \hat{V}_t + \epsilon_t, \end{aligned} \quad (1)$$

where  $\epsilon_t$  represents a noise term that can not be learned.

We employ autoregressive sparse Gaussian processes (ASGP) as the motion prediction model. An ASGP integrates an autoregressive process with a sparse Gaussian process (SPGP) using pseudo-inputs [25]. SPGP is a Gaussian process regression model whose training cost is  $O(M^2N)$  and

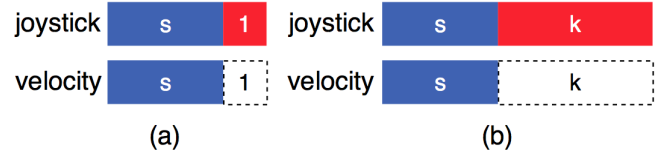


Fig. 3: **Time-series velocity prediction.** (a) Immediate velocity prediction. At time-step  $t$ , given the previous  $s$  time-steps of both joystick and velocity, and the current time-step joystick input  $J_t$ , predict the velocity  $v_t$  (the dashed part). (b) Velocity sequence prediction. Given the past  $s$  time-steps of both joystick and velocity, and the future  $k$  time-steps joystick input  $(J_t, J_{t+1}, \dots, J_{t+(k-1)})$ , predict the future  $k$  velocity  $(V_t, V_{t+1}, \dots, V_{t+(k-1)})$ .

---

#### Algorithm 1 Predicting velocity sequence.

---

**Require:** a past velocity sequence  $\{V_{t-s}, \dots, V_{t-1}\}$ .

**Require:** a past and future joystick command sequence  $\{J_{t-s}, \dots, J_{t-1}, J_t, J_{t+1}, \dots, J_{t+(k-1)}\}$ .

**Ensure:** A sequence of velocities  $\{\hat{V}_t, \hat{V}_{t+1}, \dots, \hat{V}_{t+(k-1)}\}$

- 1: seq = [ ]
  - 2: **for** i= 0 to k-1 **do**
  - 3:  $\hat{V}_{t+i} = f(\bar{X}_{t+i}, J_{t+i})$
  - 4: Update the unknown  $V_{t+i}$  with  $\hat{V}_{t+i}$  in  $\bar{X}_{t+i+1}$
  - 5: seq.push( $\hat{V}_{t+i}$ )
  - 6: **end for**
  - 7: **return** seq
- 

prediction cost is  $O(M^2)$ , where  $M$  is the number of pseudo-inputs,  $N$  is the number of training samples and  $M \ll N$ .

Algorithm 1 provides the details of the prediction process. Given an additional  $k$  time-steps of future joystick commands, the Recurrent Sliding Window method [7] uses the predicted velocity as the input for predicting the next velocity until a  $k$ -step velocity sequence is predicted (as shown in Fig. 3). The interface for velocity sequence prediction is summarized by :

$$\begin{aligned} (\hat{V}_t, \dots, \hat{V}_{t+(k-1)}) \\ = f_V(J_{t-s}, \dots, J_{t+(k-1)}, V_{t-s}, \dots, V_{t-1}) \end{aligned} \quad (2)$$

where  $\hat{V}_t, \dots, \hat{V}_{t+(k-1)}$  are the predicted velocity sequence with length  $k$ . In practice, the future joystick inputs  $J_{t+1}, \dots, J_{t+k-1}$  can be obtained from a path planner.

We will note in passing that since  $V_t = [v_t, \omega_t]^T \in \mathbb{R}^2$ , Eq. 1 actually represents two separate prediction functions:

$$\hat{v}_t = f_v(j_{t-s}, \dots, j_{t-1}, v_{t-s}, \dots, v_{t-1}, j_t) \quad (3)$$

$$\hat{\omega}_t = f_\omega(j_{t-s}, \dots, j_{t-1}, \omega_{t-s}, \dots, \omega_{t-1}, j_t) \quad (4)$$

where  $j_i$  in the two equations are the corresponding linear (for  $f_v$ ) or angular (for  $f_\omega$ ) joystick input.

Given the velocity sequence  $\{V_i\}_{i=1}^k$ , we integrate using

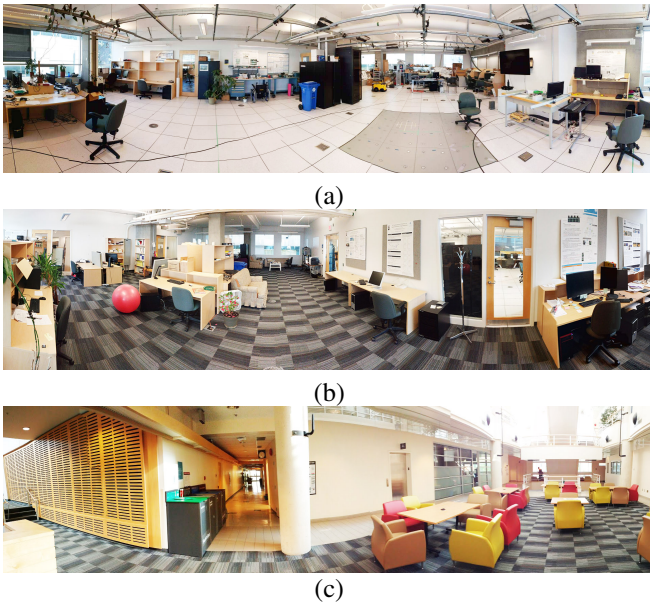


Fig. 4: **Panorama view of experimental environment.** Best viewed in color. (a) office with tiles, (b) office with carpets, (c) office with hybrid environment.

a unicycle model

$$\begin{bmatrix} \dot{x} \\ \dot{y} \\ \dot{\theta} \end{bmatrix} = \begin{bmatrix} v \cos \theta \\ v \sin \theta \\ \omega \end{bmatrix} \quad (5)$$

to obtain a corresponding pose trajectory  $\{P_i\}_{i=1}^k = \{(x_i, y_i, \theta_i)\}_{i=1}^k$ . Since discrete time data is provided, we use a trapezoidal quadrature to approximate the integral.

## V. EXPERIMENTS

In this section, we evaluate our integrated system in real-world experiments including different lighting and floor conditions.

### A. Data Collection

In the data collection stage we drive the wheelchair around our experimental environments attempting to manually generate roughly random (but safe) motions. The three indoor environments shown in Fig. 4 were used:

- 1) A lab with only tile floor.
- 2) A lab with only carpet floor.
- 3) An atrium area with both (the same) carpet and (different) tiles.

We collected data in eight ROS bags for environments 1 and 2 respectively. To evaluate our model’s performance on a complex and not previously encountered environment, two bags were collected from environment 3. Each bag contains about 20 minutes of sequential data, and the data sequences in each begin and end with the wheelchair motionless and the joystick zeroed for several seconds so that they can be concatenated in arbitrary order. In all of the analysis below

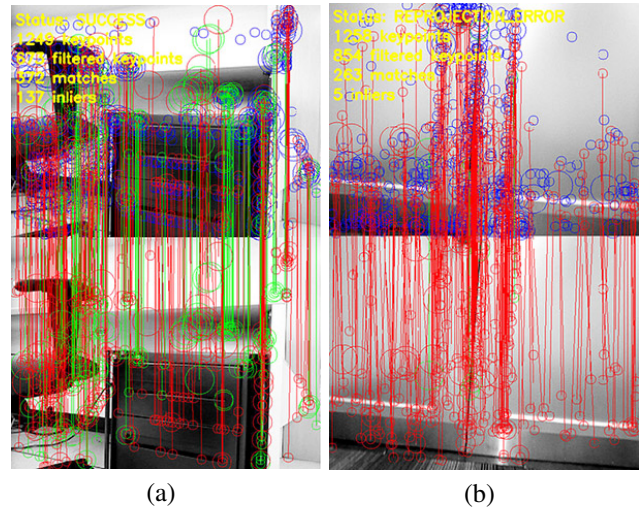


Fig. 5: **Comparison of visual odometry feature matching in rich feature space and in limited feature space.** Best viewed in color. (a) Success mode: Fovis detects sufficient inliers for feature matching and camera pose estimation. (b) Failure mode: only 5 inliers in an environment (glass door in the carpet data) are detected, and Fovis failed.

we use six bags (120 min) of data for training and two bags (40 min) for testing.

In the discrete time paradigm of ASGP, all inputs must be delivered simultaneously to the regression models. Unfortunately, the VO data arrives at a very jittery 4–7Hz whereas the joystick data arrives more consistently at roughly 30Hz. In order to provide the required simultaneous input data for the regression model we linearly interpolate the raw joystick and velocity data points and resample at 5Hz.

One added complication is that the VO provided by Fovis occasionally fails in situations where very few matching feature points are detected (see Fig. 5 for an example). During these periods, VO reports the last previous velocity, which can lead to incorrect motion estimates. In practice, we did not see any such failures lasting more than a few seconds.

### B. Model Details

In Sec. IV, we mentioned that ASGP is used to model the nonlinear mapping in Eq. 1. For the purpose of comparison on this wheelchair motion prediction problem, a Multilayer Perceptron (MLP) model similar to [26] was implemented using the Deep Learning framework Torch [4]. We used three hidden linear layers and each layer contains 30 neurons. ReLU layers are used to connect the three linear layers. The input and output are the same as ASGP. We chose a batch size of 100 to train using the Adam optimization method [14].

The hyperparameter  $s$  specifying the number of past steps available to the model in Eq. 1 was manually tuned to be  $s = 4$  for ASGP and  $s = 10$  for MLP based on results from



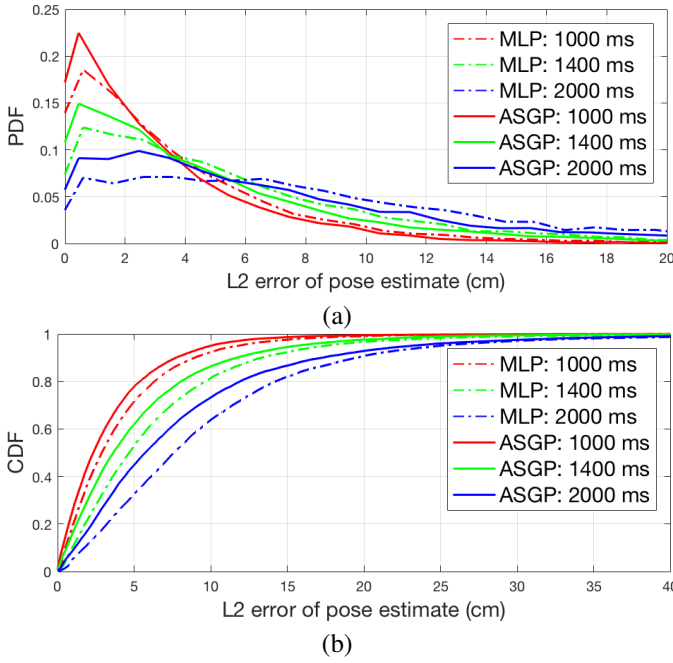


Fig. 6: PDFs and CDFs of L2 errors for position prediction at different horizons. Results are shown for models trained and tested on the tile data set, and a bin size of 1cm is used to construct the plots.

the tile training set. Finally, we manually tuned the number of pseudo-inputs used by SPGP as 20 for predicting the linear velocity and 40 for predicting the angular velocity based on results from the tile training set. Although additional pseudo-inputs continued to improve results, the benefits were marginal beyond these values and the cost (both training and evaluation) grows quadratically.

The parameter  $k$  in Eq. 1 was determined by the desired prediction horizon and the sampling frequency of 5Hz: For a horizon of 1000ms  $k = 5$ , for 1400ms  $k = 7$  and for 2000ms  $k = 10$ .

### C. Results

As discussed earlier, we train separate ASGP and MLP models to predict linear and angular velocity trajectories, and then we integrate the velocities to generate pose trajectories out to horizon  $k$ . These predicted pose trajectories are then compared with pose trajectories derived by integration of the recorded VO for the same horizon. A variety of error measurements are possible, but for reasons of space we focus on the L2 norm of the difference between the predicted  $(x, y)$  position and the recorded position.

Fig. 6 shows the PDFs and CDFs of the L2 error for position prediction over various horizons and with the two models MLP and ASGP. These results are for models trained on 120 minutes of tile data and tested on 40 minutes of tile data, but the plots are qualitatively similar for other combinations of training and testing data. As can be seen in the PDF plot, prediction accuracy degrades (the PDF

TABLE I: Percent of pose prediction with no more than 10 cm error at 1000ms horizon.

		Train (120 min)	Tile	Carpet	Both (1:1)
Test (40 min)	Tile	MLP	92.21	92.66	91.69
		ASGP	94.86	94.55	94.51
Carpet		MLP	82.21	75.26	83.45
		ASGP	83.79	82.12	82.94
Hybrid		MLP	79.96	82.04	83.46
		ASGP	84.01	83.05	82.35

becomes less peaked near zero error) as horizon increases, but in every case the ASGP models have a higher peak near zero than the corresponding MLP models.

To provide a quantitative comparison between the models for a variety of training and test data set combinations, we examine the percentage of pose predictions from the test set with error no larger than 10cm (corresponding roughly with the mapping error encountered when using common SLAM algorithms and RGB-D cameras for indoor occupancy grid construction). We will call this percentage the “success rate” of the model for a given training and test data set pair. Results are shown in Tables I, II and III for 1, 1.4 and 2 second horizons respectively. For each horizon, we train six different models: an MLP and an ASGP model using each of

- “Tile”: 120 minutes of tile data Fig. 4(a).
- “Carpet”: 120 minutes of carpet data Fig. 4(b).
- “Both (1:1)”: A combined training set with 60 minutes of tile and 60 minutes of carpet data.

We then evaluate each of the six models against three different test sets

- “Tile”: 40 minutes of tile data Fig. 4(a).
- “Carpet”: 40 minutes of carpet data Fig. 4(b).
- “Hybrid”: 40 minutes of data from the novel atrium environment Fig. 4(c) (which contains both carpet and tile).

For example, the top left value in each table corresponds to the percentage of tile test samples whose prediction error was smaller than 10cm for the MLP model trained on the tile data set. This percentage (and the corresponding ASGP percentage immediately below it) can be read from the CDF in Fig. 6 by looking at the height of the corresponding model-horizon curve where it crosses through the grid line extending vertically upward from 10cm on the horizontal axis of the plot. Turning our attention specifically to Table I, the top left cell shows that the MLP model trained on a 120 minute tile data set (Fig. 4 a) and tested on a 40 minute tile data set showed a 92.21% success rate, corresponding to approximately 11,065 test cases with L2 position estimate error (at a 1 second horizon) smaller than 10cm out of  $(40 \text{ minutes} \times 60 \text{ seconds} / \text{minute} \times 5 \text{ samples} / \text{second}) = 12,000$  test cases. This success rate can be read from the dashed red curve in Fig. 6(b).

TABLE II: Percent of pose prediction with no more than 10 cm error at 1400ms horizon.

Test (40 min)		Train (120 min)		
		Tile	Carpet	Both (1:1)
Tile	MLP	81.07	79.37	75.03
	ASGP	85.91	85.01	85.03
Carpet	MLP	67.66	50.56	69.57
	ASGP	69.40	68.72	69.66
Hybrid	MLP	63.61	63.55	67.35
	ASGP	68.50	68.73	67.72

TABLE III: Percent of pose prediction with no more than 10 cm error at 2000ms horizon.

Test (40 min)		Train (120 min)		
		Tile	Carpet	Both (1:1)
Tile	MLP	63.14	60.60	52.06
	ASGP	72.37	70.64	71.19
Carpet	MLP	43.79	31.11	51.00
	ASGP	50.21	51.69	51.69
Hybrid	MLP	40.76	41.82	43.48
	ASGP	47.91	50.89	48.77

#### D. Discussion

Tables I, II and III show that ASGP convincingly outperforms MLP for predicting future position.

Averaging across all combinations of training and test data sets, ASGP outperforms MLP by 2.14%, 5.66%, 9.73% for 1000 ms, 1400 ms and 2000 ms horizon predictions respectively, and in only two cases does MLP beat ASGP: Trained on “Both” and tested on “Carpet”, the success rate at a 1000 ms horizon of MLP is 83.45% and of ASGP is 82.94%; trained on “Both” and tested on “Hybrid”, the success rate of MLP is 83.46% and of ASGP is 82.35%. However, ASGP regains an advantage at longer horizons.

Interestingly, ASGP also seems to be more robust to variation in training data: Different training data sets do not affect the success rate for different test sets nearly as dramatically as with MLP. For example, in Table I, when tested on the tile, carpet or hybrid data sets, ASGP has a success rate of about 94%, 83% and 83% respectively, regardless of which training data set was used. The same pattern occurs in Tables II and III. Furthermore, the success rate of ASGP for testing on carpet and hybrid do not differ significantly at any fixed horizon, even though the latter is a novel environment: The success rate for testing on either carpet or hybrid at 1000 ms, 1400 ms or 2000 ms is about 83%, 68% and 50% respectively. In contrast, the success rates of various MLP models vary widely for a given test data set depending on which training data set was used.

A final observation arising from Tables I, II and III is that success rates for testing on the tile data set are consistently higher than success rates for the other two test sets. We hypothesize this result is due to better VO performance in the tile environment brought on by a combination of factors. First, the tile environment has bright artificial lighting, whereas the carpet environment has dimmer artificial lighting and the atrium has patches of strong sunlight passing

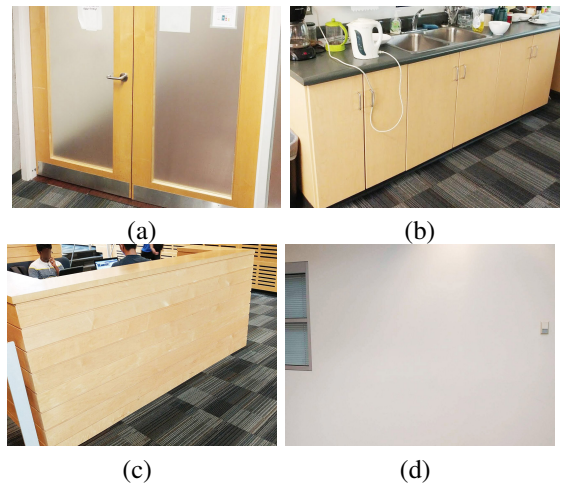


Fig. 7: Locations in the data with limited visual features. (a) and (b) are from the carpet data; (c) and (d) are from the hybrid data. In (b), the camera could only view the cabinet door, which has limited features.

through a glass wall (as shown the right side of Fig. 4 (c)), both lighting situations which can lead to limited visual features [19]. Second, the tile environment is cluttered but stable, while both the carpet and atrium environments have regions where few visual features are detected (see Fig. 7 for examples). These results again highlight the fact that VO is most effective in a rich visual environment.

## VI. CONCLUSIONS

A key step in the creation of a smart wheelchair built on a commercial powered wheelchair (PWC) platform is the ability to predict the motion of the PWC. In this paper, we presented an integrated hardware and software system to do so which requires no modifications to the PWC: We merely mount an RGB-D camera in an inconspicuous location and plug in to a standard alternative input port. We used an autoregressive sparse Gaussian process model to make pose trajectory predictions based on visual odometry and joystick data. The proposed system was evaluated on environments with different floor surfaces and different richness of visual features. Experimental results demonstrate the efficacy of our system, showing superior performance against a neural network baseline model.

## ACKNOWLEDGEMENTS

The authors would like to thank Martin Gerdzhev and Professor Joelle Pineau’s team at McGill for sharing their Arduino code and shield card to interface with the Omni+ input port, Emma Smith and Professor William C. Miller’s team at UBC for their work securing the PWC platform, and Justin Reiher and previous members of the AGEWELL WP3.2 and CanWheel engineering teams for their work on the hardware and software systems used in this research.

## REFERENCES

- [1] D. I. Anderson, J. J. Campos, D. C. Witherington, A. Dahl, M. Rivera, M. He, I. Uchiyama, and M. Barbu-Roth. The role of locomotion in psychological development. *Frontiers in psychology*, 2013.
- [2] M. Bojarski, D. Del Testa, D. Dworakowski, B. Firner, B. Flepp, P. Goyal, L. D. Jackel, M. Monfort, U. Muller, J. Zhang, et al. End to end learning for self-driving cars. *arXiv preprint arXiv:1604.07316*, 2016.
- [3] P. J. Brockwell and R. A. Davis. *Time series: theory and methods*. Springer Science & Business Media, 2013.
- [4] R. Collobert, K. Kavukcuoglu, and C. Farabet. Torch7: A matlab-like environment for machine learning. In *NIPS Workshop*, 2011.
- [5] R. A. Cooper, G. G. Grindle, J. Vazquez, J. Xu, H. Wang, J. Candiotti, C. Chung, B. Salatin, E. Houston, A. Kelleher, et al. Personal mobility and manipulation appliance design, development, and initial testing. *Proceedings of the IEEE*, 2012.
- [6] U. DeSA. World population prospects: the 2012 revision. *Population Division of the Department of Economic and Social Affairs of the United Nations Secretariat, New York*, 2013.
- [7] T. G. Dietterich. Machine learning for sequential data: A review. In *Joint IAPR International Workshops on Statistical Techniques in Pattern Recognition (SPR) and Structural and Syntactic Pattern Recognition (SSPR)*. Springer, 2002.
- [8] F. Doshi and N. Roy. Efficient model learning for dialog management. In *HRI*, 2007.
- [9] A. I. Eliazar and R. Parr. Learning probabilistic motion models for mobile robots. In *ICML*, 2004.
- [10] Z. Fang and S. Scherer. Experimental study of odometry estimation methods using rgb-d cameras. In *IROS*, 2014.
- [11] L. Fehr, W. E. Langbein, and S. B. Skaar. Adequacy of power wheelchair control interfaces for persons with severe disabilities: A clinical survey. *Journal of rehabilitation research and development*, 2000.
- [12] A. S. Huang, A. Bachrach, P. Henry, M. Krainin, D. Maturana, D. Fox, and N. Roy. Visual odometry and mapping for autonomous flight using an rgb-d camera. In *ISRR*, 2011.
- [13] C. Kerl, J. Sturm, and D. Cremers. Robust odometry estimation for rgb-d cameras. In *ICRA*. IEEE, 2013.
- [14] D. Kingma and J. Ba. Adam: A method for stochastic optimization. *ICLR*, 2015.
- [15] F. Leishman, V. Monfort, O. Horn, and G. Bourhis. Driving assistance by deictic control for a smart wheelchair: The assessment issue. *IEEE Transactions on Human-Machine Systems*, 2014.
- [16] S. Levine, C. Finn, T. Darrell, and P. Abbeel. End-to-end training of deep visuomotor policies. *Journal of Machine Learning Research*, 2016.
- [17] C. Ma, W. Li, R. Gravina, and G. Fortino. Activity recognition and monitoring for smart wheelchair users. In *CSCWD*, 2016.
- [18] L. Meng, J. Chen, F. Tung, J. J. Little, J. Valentin, and C. de Silva. Backtracking regression forests for accurate camera relocation. In *IROS*, 2017.
- [19] M. Munaro, F. Basso, S. Michieletto, E. Pagello, and E. Menegatti. A software architecture for rgb-d people tracking based on ros framework for a mobile robot. *Frontiers of Intelligent Autonomous Systems*, 2013.
- [20] D. Nistér, O. Naroditsky, and J. Bergen. Visual odometry. In *CVPR*, 2004.
- [21] D. Scaramuzza and F. Fraundorfer. Visual odometry [tutorial]. *Robotics & Automation Magazine, IEEE*, 2011.
- [22] D. Schwesinger, A. Shariati, C. Montella, and J. Spletzer. A smart wheelchair ecosystem for autonomous navigation in urban environments. *Autonomous Robots*, 2017.
- [23] A. Segal, D. Haehnel, and S. Thrun. Generalized-icp. In *RSS*, 2009.
- [24] R. C. Simpson. Smart wheelchairs: A literature review. *Journal of rehabilitation research and development*, 2005.
- [25] E. Snelson and Z. Ghahramani. Sparse gaussian processes using pseudo-inputs. In *NIPS*, 2006.
- [26] P. TalebiFard, J. Sattar, and I. M. Mitchell. A risk assessment infrastructure for powered wheelchair motion commands without full sensor coverage. In *IROS*, 2014.
- [27] P. Viswanathan, E. P. Zambalde, G. Foley, J. L. Graham, R. H. Wang, B. Adhikari, A. K. Mackworth, A. Mihailidis, W. C. Miller, and I. M. Mitchell. Intelligent wheelchair control strategies for older adults with cognitive impairment: user attitudes, needs, and preferences. *Autonomous Robots*, 2017.
- [28] H. Xu, Y. Gao, F. Yu, and T. Darrell. End-to-end learning of driving models from large-scale video datasets. *CVPR*, 2017.